scientific reports

Check for updates

OPEN

Numerical simulation of cable sheath damage detection based on torsional mode guided wave

He Zhu, Cheng Liu✉, Zhaobing Han, Yue Zhang & Wenlong Chen

In view of the cracking, sag, and damage of sheath caused by the load effect and external force impact of power cable, the echo parameters of cable sheath damage detection based on the characteristics of torsional guided wave propagation are studied in this work. According to the Navier displacement equilibrium equation, the dispersion curve of a magnetostrictive guided wave of the cable sheath was solved, and the T(0,1) mode with a group velocity of 1198.8 m/s and no dispersion was selected. Furthermore, while considering the excitation frequency, loss rate, and direction of the damaged section, the displacement field and the echo characteristic parameters of guided wave in the cable sheath were solved. Moreover, by analyzing the time-domain signals of damaged section echo, the cubic fitting function for the loss rate of the damaged section and the damaged section echo coefficient were obtained, which can effectively characterize the quantitative relationship between the damaged location, size, and guided wave echo of the cable sheath.

Keywords Cable sheath, Damage parameters, Echo wave, Guided wave, Torsional mode

There are many problems with today's transmission lines[1,2]. During operation, the sheath of power cable can be cracked, dented, and damaged due to load effects and external force impacts such as damp corrosion, medium aging, or improper construction operation[3]. Magnetostrictive ultrasonic guided waves encounter the boundary and variable cross-section in the process of medium propagation, causing reflection, transmission, and mode conversion, and are sensitive to small damage[4]. Based on this characteristic, ferromagnetic materials are generally used to couple the guided wave into cable sheath to deform and propagate it towards both ends in the form of a guided wave. Any damage in the cable sheath can be detected by analyzing the change in the guided wave echo signal. ()

Magnetostrictive guided wave detection technology has been widely used in the detection of industrial pipelines and steel rods[5–10]. Furthermore, a few scholars have also conducted relevant research on the application of this technology in power engineering. In Refs.[11–15], the magnetostrictive guided wave dispersion equation in the ferromagnetic components is solved, and the guided wave excitation process is modeled and analyzed. Among them, Zhou[11] excited the guided wave of L(0,1)mode and verified the theoretical model. The results show that the amplitude of magnetostrictive guided wave is related to the magnetostrictive force. Progressively, Yang, Pengfei, and others[12–14] studied the magnetic coupling process of magnetostrictive guided wave force. The reported results indicate that the coupling coefficient is related to the change rate of static magnetic field. Based on Refs.[12–14], Gan[15] analyzed the modal and dispersion characteristics of a low-frequency longitudinal guided wave, compared and analyzed the damage of through-hole and transverse grooved pipeline using L(0,1) modal guided wave, and obtained the relationship between damage reflection coefficient and structural section loss coefficient. However, the magnetic coupling characteristics of magnetostrictive guided wave force in T(0,1) torsional mode were not analyzed and calculated. In Refs.[16–19], the coupling process of magnetostrictive guided wave in the cable structure was studied, and the guided wave detection of cable structural defects is simulated and verified by finite element method. Cao et al.[16] studied the propagation characteristics of magnetostrictive guided wave in aluminum cable sheaths, such as multimode, dispersion, and attenuation, by establishing a simplified model of aluminum cable sheath and solving its dispersion equation, and obtaining the corresponding dispersion curve. Relying on a simplified model for aluminum cable sheath established in Ref.[15], Zhou et al.[17] equivalent the cable aluminum sheath to bellows without considering the spiral angle of aluminum sheath. Using 32 kHz T(0,1) mode magnetostrictive guided wave, the sheath damage with a cross-section accounting for more than 4.25% of the aluminum cable sheath can be detected; The propagation distance of T(0,1)mode is long and the attenuation is slow. However, with the increase of propagation distance, the reflection of torsional wave on

School of Civil Engineering and Architecture, Northeast Electric Power University, Jilin City 132012, China. ✉email: 2535662712@qq.com

small defects decreases and the signal-to-noise ratio of detection signal also decreases. Mehmetk et al.[18] pointed out that the dispersion simulation of magnetostrictive guided wave in a buried cable medium is represented by a simple harmonic wave in the propagation direction, where the node displacement can be solved by discretization of the guided wave section, nevertheless, this method does not demonstrate whether it has a faster convergence than the finite element method. Furthermore, Yang et al.[19] conducted guided wave detection on a healthy cable core with complete structure and manually set the damaged cable core, and found that the healthy cable guided wave packet did not diffuse significantly, while the guided wave reflected the end echo signal at the damaged sheath. However, this echo is multimodal, accompanied by a large number of noise signals, wave packet aliasing, and difficult to control test variables, and therefore, the obtained data is not conducive to acquisition.

According to the above mentioned research on magnetostrictive guided wave field and damage echo characteristics of the cable sheath, there exist the following technical gaps that need to be bridged: in the establishment of mathematical model, although the factors such as excitation frequency, guided wave mode, structural parameters, and guided wave attenuation are considered, the influence of nonlinear effect of material is ignored, and the mathematical model still adopts a two-dimensional model. The solution process is generally progressed by simplifying the boundary effect between the structures, and there are many assumptions, hence there is a large deviation from the actual situation. Additionally, the difference and trend of guided wave displacement field of torsional mode under the complex damage state parameters in practical engineering are not considered. In view of the above shortcomings, the magnetostrictive guided wave field and damage echo characteristics of cable sheath are studied in this work. Firstly, the constitutive model of magnetostrictive effect under magnetic force coupling is derived. The motion equation of the guided wave in cable sheath material is established according to the Navier displacement balance equation. Here, the time resonant displacement vector is decomposed by Helmholtz, and the modal dispersion curve is solved by a semi-analytical finite element numerical method. In addition, the torsional mode guided wave excitation model and the three-dimensional model of damaged cable sheath are built. By changing the excitation frequency, the loss rate of damaged section, and direction of damaged section of cable sheath, the variation in magnetostrictive guided wave displacement field in cable sheath under the influence of multiple parameters is analyzed. Lastly, by analyzing the displacement time domain signal of the echo of damaged section, the quantitative relationship between the damaged position and size of cable sheath and the guided wave excitation is studied.

Propagation characteristic equation of magnetostrictive guided wave in cable sheath

Magnetostrictive effect force magnetic coupling elastic constitutive mode

According to the deformation mode of the material, the magnetostrictive guided wave is divided into bending mode (radial displacement component, axial displacement component and circumferential displacement component), torsion mode (only circumferential displacement component) and longitudinal mode (only circumferential displacement component and radial displacement component).

Assuming that the magnetostrictive materials are magnetically isotropic, then according to the basic principle of magnetostriction[20], the magnetostrictive coefficient or strain of magnetostrictive materials under the action of external magnetic field H is given by Eq. (1).

$$\varepsilon = \lambda = \frac{3\lambda_S}{2M_S^2}(\mu_r - 1)^2 H^2 \tag{1}$$

where Eq. (1): ε-the strain of material, dimensionless; λ-the magnetostrictive coefficient, ppm; λ_S-the saturation magnetostrictive constant, which is related to the material; M_S-the saturation magnetization, A/m; H-the applied magnetic field, A/m; μ_r-the relative permeability, dimensionless.

Equation (1) reflects the relationship between the internal strain of material and the magnetic field strength, essentially indicating that the change in applied magnetic field ΔH will cause a change in the internal strain of the magnetostrictive material Δε, When the frequency of external applied magnetic field H changes significantly, owing to various problems such as strain lag effect in the material, the changes in strain field and external magnetic field are inconsistent, and consequently, the stress field generated in the material propagates in the tested specimen in the form of a stress wave.

Dispersion equation of magnetostrictive guided wave motion in cable sheath

According to the principle of elasticity, during the propagation of guided wave, the particle displacement satisfies the Navier displacement balance equation[21]. For the displacement balance equation in an isotropic elastic medium, see Eq. (2).

$$\mu\nabla^2\overline{u} + (\lambda + \mu)\nabla(\nabla \cdot \overline{u}) = \rho\left(\frac{\partial^2\overline{u}}{\partial t^2}\right) \tag{2}$$

where: $\overline{u}$-the displacement vector; ρ-the material density; λ-the lame constant; μ is the shear modulus; ∇^2-the Laplace operator; ∇-the gradient operator. Using Helmholtz decomposition theorem, the displacement vector $\overline{u}$ can be decomposed into a compressible scalar potential ϕ Constant volume vector function ψ. See Eq. (3).

$$\begin{cases} \overline{u} = \nabla \cdot \phi + \nabla \times \psi \\ \phi \times \psi = 0 \end{cases} \tag{3}$$

where ϕ and ψ-the scalar potential and vector potential, respectively.

Substitute Eq. (3) into Navier displacement balance Eq. (2), and simplify to obtain Eq. (4).

$$\nabla\left[(\lambda+2\mu)\nabla^2\phi-\rho\frac{\partial^2\phi}{\partial t^2}\right]+\nabla\left[\mu\nabla^2\psi-\rho\frac{\partial^2\psi}{\partial t^2}\right]=0 \tag{4}$$

If Eq. (4) is true, it is necessary to make both of them zero, and then Eqs. (5) and (6) are obtained.

$$C_L^2\nabla^2\phi=\frac{\partial^2\phi}{\partial t^2} \tag{5}$$

$$C_T^2\nabla^2\psi=\frac{\partial^2\psi}{\partial t^2} \tag{6}$$

where, C_L-the group velocity of the material, m/s, $C_L=\sqrt{(\lambda+2\mu)/\rho}$; C_T-the Phase velocity of the materials, m/s,$C_T=\sqrt{\mu/\rho}$.

The cable sheath is assumed to be an infinitely long tube, and the cylindrical coordinate system is used to simplify the propagation of guided waves in the tube. Let the z-axis along the cable axis perpendicular to the radius direction to establish the cylindrical coordinate system, as shown in Fig. 1.

Then the displacement equation of the magnetostrictive guided wave in the infinite tube is Eq. (7).

$$\begin{aligned}&(\lambda+2\mu)\tfrac{\partial\phi}{\partial r}-\tfrac{2\mu}{r}\tfrac{\partial\omega_z}{\partial\theta}+2\mu\tfrac{\partial\omega_\theta}{\partial z}=\rho\tfrac{\partial^2u_r}{\partial t^2}\\&(\lambda+2\mu)\tfrac{1}{r}\tfrac{\partial\phi}{\partial\theta}-2\mu\tfrac{\partial\omega_r}{\partial z}+2\mu\tfrac{\partial\omega_z}{\partial r}=\rho\tfrac{\partial^2u_\theta}{\partial t^2}\\&(\lambda+2\mu)\tfrac{\partial\phi}{\partial z}-\tfrac{2\mu}{r}\tfrac{\partial(r\omega_\theta)}{\partial z}+2\mu\tfrac{\partial\omega_z}{\partial\theta}=\rho\tfrac{\partial^2u_z}{\partial t^2}\end{aligned} \tag{7}$$

In Eq. (7):

$$\begin{cases}\phi=\dfrac{1}{r}\dfrac{\partial(ru_r)}{\partial r}+\dfrac{1}{r}\dfrac{\partial u_\theta}{\partial\theta}+\dfrac{\partial u_z}{\partial z}\\2\omega_r=\dfrac{1}{r}\dfrac{\partial u_z}{\partial\theta}-\dfrac{\partial u_\theta}{\partial z}\\2\omega_\theta=\dfrac{\partial u_r}{\partial z}-\dfrac{\partial u_z}{\partial r}\\2\omega_r=\dfrac{1}{r}\left[\dfrac{\partial(ru_\theta)}{\partial r}-\dfrac{\partial u_r}{\partial\theta}\right]\end{cases} \tag{8}$$

where, u_r, u_θ, u_z-radial displacement, circumferential displacement and axial displacement of cable sheath particles, m;$\omega_r, \omega_\theta, \omega_z$-three different components of the rotation vector;ϕ-the volume constant of cylindrical coordinates;r-cylindrical radius;θ-cylindrical section angle.

Semi-analytical finite element method to solve guided wave modal dispersion equation and modal selection

The material of the detected cable section is uniform, isotropic and not affected by external forces. When the surrounding environment of the cable section is air, there is no displacement limit on the outer surface, and the radial stress σ_{rr} and two shear stresses $\sigma_{r\theta}$ and σ_{rz} on the surface are zero.

Equation (9) is obtained from the stress–strain relationship, namely Hooke's law.

$$\begin{cases}\sigma_{rr}=\lambda\phi+2\mu\dfrac{\partial u_r}{\partial r}\\\sigma_{r\theta}=\mu\left(\dfrac{1}{r}\dfrac{\partial u_r}{\partial\theta}+r\dfrac{\partial}{\partial r}\left(\dfrac{u_\theta}{r}\right)\right)\\\sigma_{rz}=\mu\left(\dfrac{\partial u_r}{\partial z}+\dfrac{\partial u_z}{\partial r}\right)\end{cases} \tag{9}$$

The guided wave medium is isotropic viscoelastic material. Assuming that the guided wave displacement field in the propagation direction is in the simple harmonic form, the simple harmonic vibration equation of the guided wave is derived from the sheath stress boundary condition in the cylindrical coordinate system as Eq. (10).

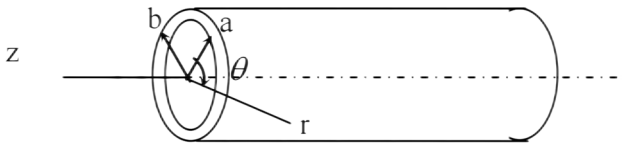

Figure 1. Infinite circular tube model in cylindrical coordinates.

$$\begin{cases} u_r = U_r(r)\cos(n\theta)\cos(\omega t + kz) \\ u_\theta = U_0(r)\sin(n\theta)\cos(\omega t + kz) \\ u_z = U_z(r)\cos(n\theta)\cos(\omega t + kz) \end{cases} \tag{10}$$

where ω-angular frequency, rad/s; k-wavenumber; n-the value of n-circumferential order is n = 0, 1, 2, 3,….

When n = 0 is an axisymmetric mode, there are only radial and axial vibrations, namely the longitudinal propagation mode L (0, m) and the torsional propagation mode T (0, m); when n = 1,2,3… is a non-axisymmetric mode, which contains three displacement components in the direction of the cylindrical coordinate axis, that is, the bending propagation mode F (n, m); ur, uθ, and uz represent radial displacement, circumferential displacement, and axial displacement components, respectively. Ur, Uθ, Uz are the corresponding displacement amplitudes composed of Bessel function or modified Bessel function depending on the amplitude angle[22].

The torsional wave case needs to meet the condition of Eq. (11).

$$\mathrm{u_r} = 0,\ \mathrm{u_z} = 0 \tag{11}$$

Integrated Eqs. (7), (10), (11), get Eq. (12).

$$u_\theta = \frac{1}{\beta} B J_1(\beta r) e^{i(kz - wt)} \tag{12}$$

The dispersion coefficient in Eq. (12):

$$\beta^2 = w^2\left(\frac{1}{c_T^2} - \frac{1}{c_p^2}\right).$$

According to the relationship between stress and strain, strain and displacement, the solution of the stress field is Eq. (13).

$$\begin{cases} \sigma_{rr} = \left\{-\lambda\left(\alpha^2 + k^2\right)f + 2\mu\left[f'' + \frac{n}{r}\left(g_3' - \frac{g_3}{r}\right) + kg_1'\right]\right\}\cos n\cos(\omega t + kz) \\ \sigma_{r\theta} = \mu\left\{-\frac{2n}{r}\left(f' - \frac{f}{r}\right) - \left(2g_3'' - \beta^2 g_3\right) - k\left(\frac{n+1}{r}g_1 - g_1'\right)\right\}\sin n\theta\cos(\omega t + kz) \\ \sigma_{rz} = \mu\left\{-2kf' - \frac{n}{r}\left[g_1' + \left(\frac{n+1}{r} - \beta^2 + k^2\right)g_1\right] - \frac{nk}{r}g_3\right\}\cos n\theta\sin(\omega t + kz) \end{cases} \tag{13}$$

The Eq. (11) of the boundary conditions under the ideal state of the model is substituted into the Eq. (13) to calculate the Eq. (14).

$$[D]_{6\times6}\begin{bmatrix} A & B & A_1 & B_1 & A_2 & B_2 \end{bmatrix}^T = \begin{bmatrix} 0 & 0 & 0 & 0 & 0 & 0 \end{bmatrix}^T \tag{14}$$

Solving the motion equation of the guided wave in the cable sheath is finally reduced to solving the dispersion equation of Eq. (14). When Eq. (14) has solutions other than 0, let $[D]_{6\times6}$=0, obtain Eq. (15).

$$D = \begin{bmatrix} c_{11} & c_{12} & c_{13} & c_{14} & c_{15} & c_{16} \\ c_{21} & c_{22} & c_{23} & c_{24} & c_{25} & c_{26} \\ c_{31} & c_{32} & c_{33} & c_{34} & c_{35} & c_{36} \\ c_{41} & c_{42} & c_{43} & c_{44} & c_{45} & c_{46} \\ c_{51} & c_{52} & c_{53} & c_{54} & c_{55} & c_{56} \\ c_{61} & c_{62} & c_{63} & c_{64} & c_{65} & c_{66} \end{bmatrix} = 0 \tag{15}$$

Equation (15) is cable sheath's dispersion equation of guided wave propagation. When the guided wave order n is zero, its solution is an axisymmetric guided wave mode. Equation (15) can be decomposed into a form of the product of fourth-order determinant and second-order determinant. See Eq. (16).

$$D = D_1 \cdot D_2 = 0 \tag{16}$$

Namely:

$$D_1 = \begin{bmatrix} c_{11} & c_{13} & c_{14} & c_{16} \\ c_{31} & c_{33} & c_{34} & c_{36} \\ c_{41} & c_{43} & c_{43} & c_{43} \\ c_{61} & c_{63} & c_{63} & c_{63} \end{bmatrix} = 0 \tag{17}$$

$$D_2 = \begin{bmatrix} c_{23} & c_{25} \\ c_{53} & c_{55} \end{bmatrix} = 0 \tag{18}$$

The dispersion curves of longitudinal mode and torsional mode in the sheath are obtained by solving the determinant D1 = 0 and D2 = 0. cij is the Bessel function of the inner and outer diameters a, b, Lame constant λ, material density ρ, angular frequency ω and guided wave number k of the cable sheath.

Both Eqs. (17) and (18) contain Bessel function, which belongs to transcendental equation and cannot directly solve the exact solution. Therefore, the Matlab program is built to solve the approximate solution by semi-analytical finite element numerical method. The solving process is:

(1) A two-dimensional discrete model of the circumferential section of the cable sheath is established by comprehensively scanning the required area in a grid format, as shown in Fig. 2.
(2) When discrete analysis is carried out, the cross-sectional area of the circumferential infinite element is denoted as Ω, and the cross-section is discretized by one-dimensional four-node element. The discrete element is denoted as Ωg, and the number of discrete guided wave medium cross-section elements is denoted as Ωgi.
(3) The element stiffness matrix is calculated by domain integral. According to the anisotropy and frequency domain characteristics of viscoelastic materials, the average value of real strain energy with respect to time is obtained, and the imaginary part is the loss of energy. Through the relationship between frequency and mode, the strain energy part and the kinetic energy part are substituted into the Hamiltonian equation.
(4) According to the arbitrariness of the global vector δU of the unknown node displacement, the wave equation of the homogeneous medium is obtained. The imaginary part of the wave equation is eliminated by the linear matrix T, and a new node displacement vector is obtained. The characteristic equation is obtained by solving the non-zero solution, so as to obtain the characteristic solutions of ξ and ω.
(5) The characteristic equation is simplified into a real symmetric matrix equation by using matrix T, and then the propagation mode is obtained by solving ω(ξ) through the standard characteristic vector problem.
(6) Given a wave value, the zero solution of the characteristic matrix is obtained, and the value of the frequency is obtained. The relationship between the wave velocity and the frequency is solved, and the dispersion characteristic curve is drawn.

Set the cable sheath inner and outer diameter a, b, material density ρ, Young's modulus E, Poisson 's ratio μ, as shown in Table 1. The group velocity and phase velocity dispersion characteristic curves of the model are obtained as Fig. 3.

From Fig. 3, the frequency range of the given excitation alternating current is 0–200 kHz, and the order of the circumferential displacement vector of the longitudinal L mode and the torsional T mode is 0. The group velocity dispersion curve of the L-mode guided wave has five kinds of modulus in the range of 0–200 kHz, and each modulus is excited at 5.363 kHz, 76.35 kHz, 147.2 kHz, and 177.9 kHz, respectively. The group velocity dispersion curve of the T-mode guided wave has three kinds of modulus in the range of 0–200 kHz, and each modulus is excited at frequencies of 0 kHz, 75.74 kHz, and 150.8 kHz, respectively. Therefore, the dispersion phenomenon of the torsional T mode in the range of 0–200 kHz is less, which is beneficial to the excitation of a single mode guided wave.

In order to realize the effective detection of cable sheath damage and the low signal-to-noise ratio propagation of guided waves, it is necessary to select the guided wave mode with more stable group velocity, that is, the wave velocity should be kept as consistent as possible when the frequency changes. The T (0,1) mode of Figs. 2, 3, 4, 5, 0–200 kHz and the L (0,1) mode after 76.67 kHz meet the requirements, but the L mode will excite three modes of L mode guided waves in the same frequency band. In the frequency range of 0–75.74 kHz, the torsional T-mode guided wave will only excite the T (0,1) mode with a single modulus and stable group velocity, and the calculated group velocity of this mode is 1198.8 m/s.

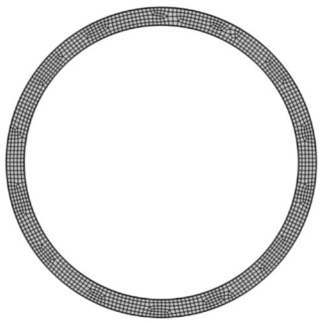

Figure 2. Two-dimensional discretization model of cable sheath section.

Parameter name	Parameter value
Inner diameter/mm	30.3
Outer diameter/mm	30.4
Density/kg m^{-3}	480
Young's modulus/GPA	1.9
Poisson's ratio	0.38

Table 1. Material parameters of 110 kV YJLW03-Z high voltage cable sheath.

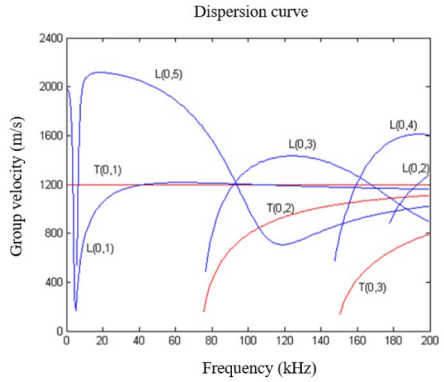

(a) Group velocity.

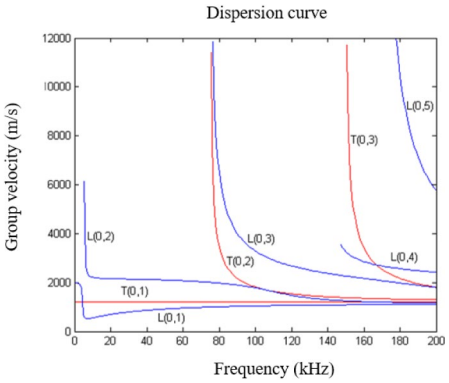

(b) Phase velocity

Figure 3. Dispersion curves of L-mode and T-mode guided waves. (**a**) Group velocity. (**b**) Phase velocity.

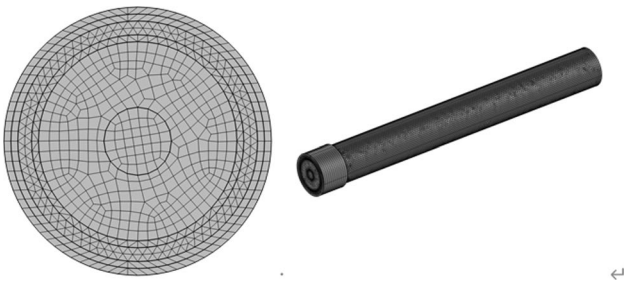

Figure 4. Model meshing diagram.

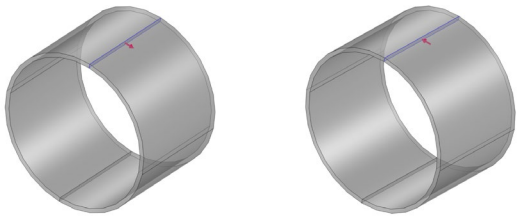

(a) magnetization direction (b) excitation orientation

Figure 5. Magnetization and excitation direction. (**a**) Magnetization direction. (**b**) Excitation orientation.

According to the dispersion curve, the torsional T-mode guided wave is selected for the magnetostrictive guided wave mode used for cable sheath damage detection. The modulus is T (0, 1) and the frequency range is 0–75.74 kHz.

Cable sheath magnetostrictive torsional mode guided wave detection simulation model

Cable sheath torsional mode guided wave detection model and meshing

COMSOL is one of the leading commercial finite element analysis software widely used at present. There are many successful application cases in the cross field of guided wave damage detection[23,24]. The finite element model of torsional mode guided wave detection of cable sheath is established. The model is mainly composed of the following four parts : the Fe–Ni alloy strip that excites the magnetostrictive effect, the annular AC coil that provides the alternating excitation current, the cable sheath to be tested, and the air domain. The geometric dimensions and model meshing of 110 kV YJLW03-Z power cable for torsional mode guided wave detection are shown in Table 2 and Fig. 4.

When the time step is selected, the time step t_step is set to be less than 1/10 of the alternating excitation current period T. When the torsional mode is excited by 40 kHz frequency, the period is 25 μs and the time step is set to 2.5 μs. The total calculation timeIn order to ensure that when the guided wave pulse echo is used to detect the damage of the cable sheath, at least one echo signal of the T (0,1) guided wave mode is received, and the total numerical simulation calculation time should meet Eq. (19).

$$T \geq \frac{2l}{C_g} \tag{19}$$

where, l-length of cable segment, m; C_g-T(0,1) guided wave group velocity at excitation frequency, m/s.

When the frequency f is 40 kHz, T > 100.1 μs is calculated, and the total calculation time is 120 μs.

Verification of magnetization direction of bias magnetic field and alternating magnetic field

Firstly, the Fe–Ni alloy ribbon is magnetized along the circumferential direction according to the direction indicated by the arrow in Fig. 5a. Since the AC coil is closed, a circumferential section of the coil is arbitrarily selected, and the AC electrical signal is introduced in the direction of the arrow in Fig. 5b.

The bias magnetic field is calculated by steady state, and the Fe–Ni alloy strip generates a circumferentially distributed magnetic field at a preset magnetization intensity, as shown in Fig. 6.

The excitation signal is used as the dynamic input variable of the sensor. In order to avoid the interference of multiple excitation waveforms on the waveform analysis received by the guided wave, a periodic excitation signal is selected. In this paper, the sinusoidal signal function modulated by Hanning window is selected, see Eq. (20).

Conductor		Insulation thickness (mm)	Thickness of aluminum sleeve (mm)	Thickness of outer sheath (mm)	Outside diameter (mm)
Nominal cross section (mm^2)	Approximate outer diameter (mm)	19.0	2.0	4.0	83.3
240	18.6				

Table 2. Geometric dimensions of 110 kV YJLW03-Z cable.

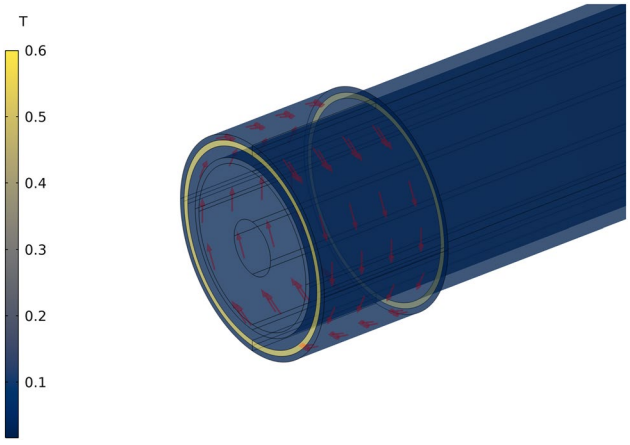

Figure 6. Magnetic field distribution of Fe–Ni alloy ribbons under circumferential magnetization.

$$i(t) = 0.5\left[1 - \cos(\frac{2\pi ft}{6})\right]\sin(2\pi f)(t \leq \frac{6}{f}) \tag{20}$$

The excitation signal is an alternating current with a frequency of 40 kHz, a period number of 6, and an amplitude of 1A. Figures 7 and 8 is the time domain curve of the excitation signal and the frequency domain curve after Fourier transform.

As a part of the excitation magnetostrictive effect, the Fe–Ni alloy strip will produce a static bias magnetic field due to magnetization and magnetic concentration under the action of an external magnetic field. At this time, the Fe–Ni alloy strip will produce a magnetostrictive strain variation under the action of an alternating magnetic field, and its direction is determined by the direction of the bias magnetic field. The amplitude of the magnetostrictive strain is related to the slope of the magnetostrictive B-H curve. The B-H curve of the Fe–Ni alloy strip is shown in Fig. 9.

As the magnetization of the bias magnetic field increases, the magnetic flux density of the Fe–Ni alloy material gradually increases. The slope of the B-H curve decreases significantly when the residual flux density of the Fe–Ni alloy strip exceeds 0.6 T. The magnetization of the Fe–Ni alloy strip is set to 25–300 kA/m, respectively. A section of the XY plane along the Z-axis direction at the joint of the Fe–Ni alloy strip and the cable sheath is selected. The curve of the circumferential magnetic flux density on the line segment with the magnetic field strength is calculated, as shown in Fig. 10. The residual magnetic flux density and loss under different magnetization are shown in Fig. 11.

From Figs. 10 and 11, as the magnetization of the bias magnetic field increases, the magnetic flux density of the Fe–Ni alloy band gradually increases. Under the magnetization of the circumferential magnetic field, the magnetic flux density of the axial central section of the Fe–Ni alloy strip reaches the maximum value. Due to the magnetic flux loss at the interface between the magnetic field and the air, the magnetic flux density at the edge of the Fe–Ni alloy strip is attenuated at 5 mm.When the magnetization of the bias magnetic field is 300kA/m, the maximum magnetic flux density at the center of the surface of the Fe–Ni alloy strip reaches 0.6439 T. With the increase of magnetization, the loss of magnetic flux density becomes larger and larger, so it is not appropriate to

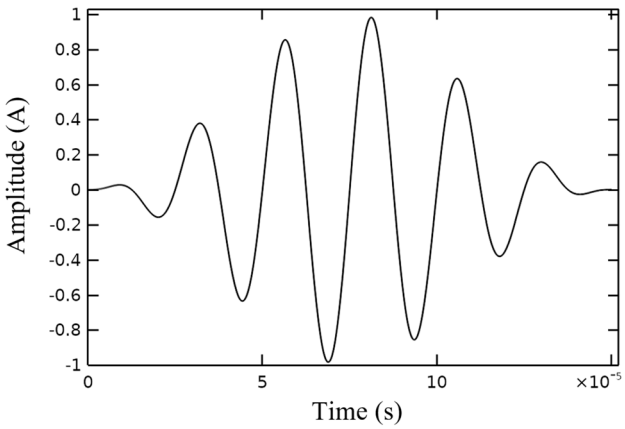

Figure 7. Excitation current time domain signal.

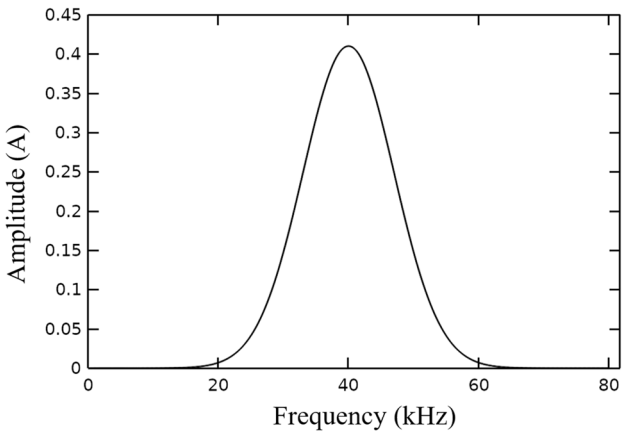

Figure 8. Excitation current frequency domain signal.

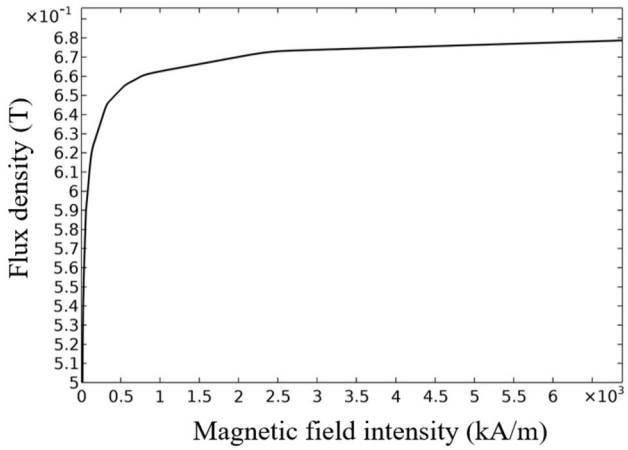

Figure 9. B-H curve of Fe–Ni alloy.

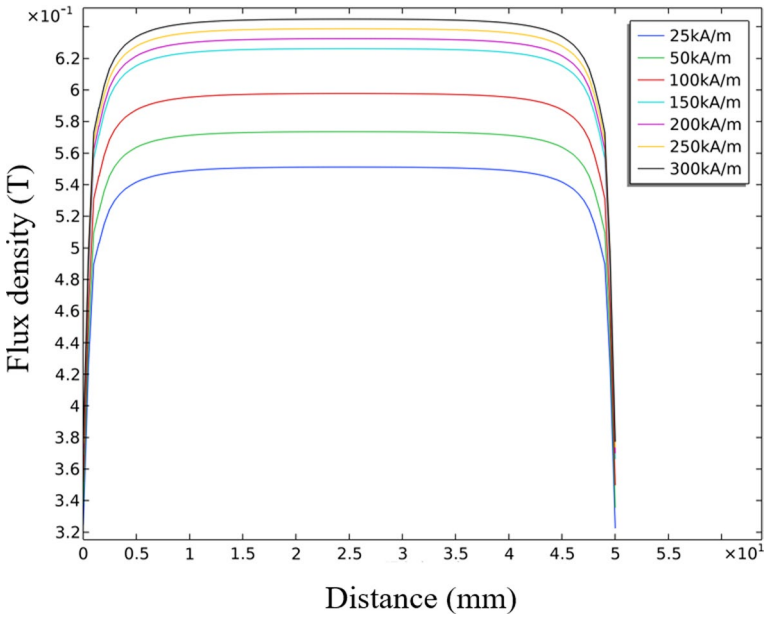

Figure 10. The magnetic flux density distribution of Fe–Ni alloy ribbons under different magnetizations.

choose too large magnetization in the static magnetic field of Fe–Ni alloy strip. The magnetization intensity is 150 kA/m, and the residual flux density is 0.6252 T.

According to the right hand rule, the magnetic field generated by the ring excitation coil should be distributed along the axial direction. The central particle near the coil on the Fe–Ni alloy strip is taken as the research object. The one-dimensional image of the magnetic induction intensity of the particle under the alternating magnetic field is shown in Fig. 12.

The distribution of the magnetic induction intensity in the Fe–Ni alloy strip is as shown in Fig. 13 when the magnetic induction intensity reaches the peak under the alternating magnetic field.

From Figs. 12 and 13, the magnetic flux density through the particle in the axial direction is the largest, and the maximum amplitude value is 1.08×10^{-3} T. Along the radial direction and circumferential direction are 3.79×10^{-9} T and 0 T, respectively, which is negligible. In line with the law of AC coil magnetic field generation. Therefore, the dynamic magnetic field excited by the coil is distributed along the axial direction of the Fe–Ni band. Because the magnetic flux density of the circumferential bias magnetic field formed by the Fe–Ni ribbon is 0.6252 T, which is much larger than the alternating axial magnetic field generated by the coil, the coupling effect of the dynamic magnetic field and the static bias magnetic field only forms the circumferential magnetization of the Fe–Ni alloy ribbon.

Verification of torsional modal guided wave modal characteristics of cable sheath

When the alternating magnetic field reaches the peak, the strain distribution of the Fe–Ni alloy strip under the excitation of the AC coil through the magnetostriction force magnetic coupling is shown in Fig. 14.

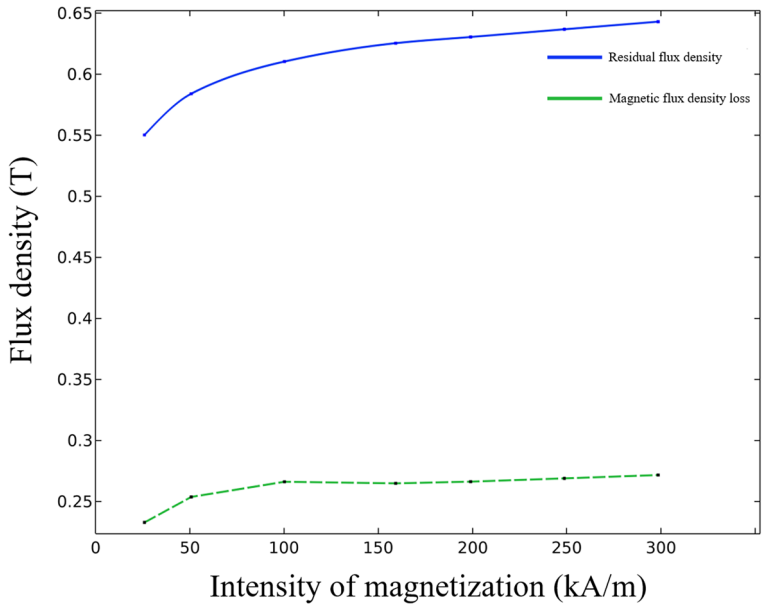

Figure 11. Magnetic flux density and loss under different magnetization intensity.

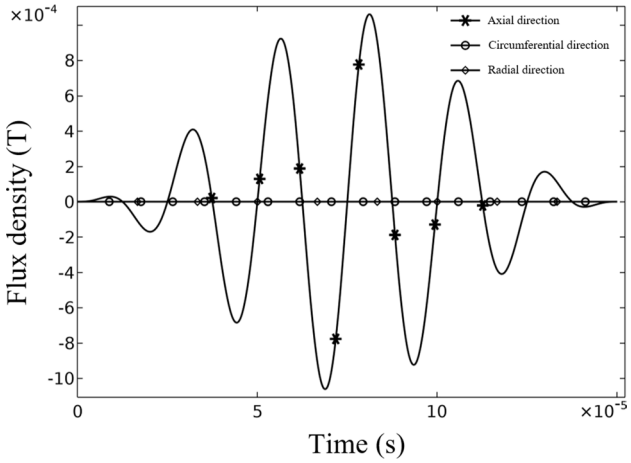

Figure 12. Magnetic flux density of particle in alternating magnetic field.

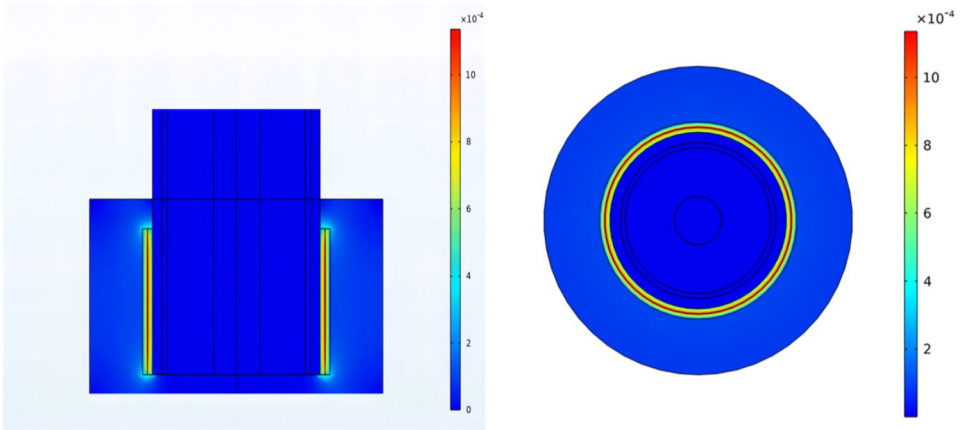

Figure 13. Magnetic flux density distribution of Fe–Ni alloy ribbons under dynamic magnetic field.

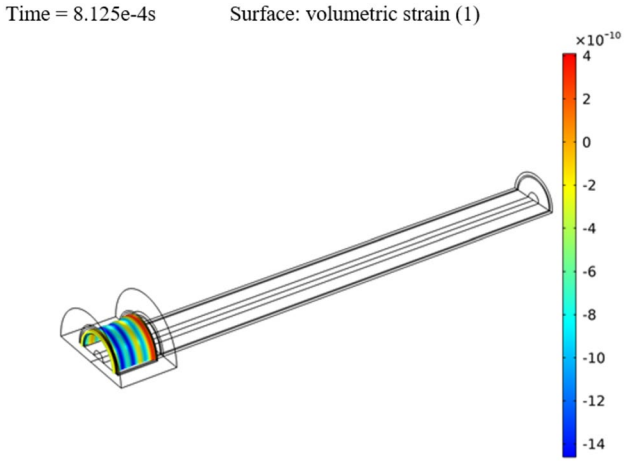

Figure 14. Strain distribution of Fe–Ni alloy strip under dynamic magnetic field.

According to Fig. 14, the Fe Ni alloy belt is subjected to transient deformation at the original position in the axial and circumferential directions, where the maximum volumetric strain is 4.0967×10^{-10}, the minimum volumetric strain is 14.1356×10^{-10}, and the magnetostrictive strain is 1.8232×10^{-9}. Under the joint action of magnetostrictive tape and AC coil, the torsional mode guided wave signal is excited in the cable sheath, and its time domain displacement curve is shown in Fig. 15.

From Fig. 15, under the excitation of the bias magnetic field magnetic flux density of 0.6252 T, the frequency of 40 kHz, and the amplitude of 1A, the maximum amplitude of the circumferential displacement component of the particle is 1.0738×10^{-8} mm, and the maximum amplitude of the axial displacement component is 1.1307×10^{-9} mm, with a difference of one order of magnitude. The guided wave generated by the excitation is mainly circumferential vibration, and the generated stress wave propagates along the axial direction of the sheath. The propagation direction is perpendicular to the direction of particle vibration, indicating that the torsional mode magnetostrictive guided wave simulated by the force-magnetic multi-field coupling can be obtained through this simulation analysis.

The guided wave vibration displacement signal is used as input, and loaded into the cable sheath end face area below the excitation coil, and the wave field of the guided wave in the cable sheath under the excitation is calculated. The stress field and displacement field distribution inside the cable sheath at different times are calculated as shown in Fig. 16.

From Fig. 16, under the excitation of alternating magnetic field, the Fe–Ni alloy strip produces magnetostrictive strain, and the magnetostrictive force is coupled on the sheath to vibrate the particles in the sheath. The incident T(0,1) mode guided wave propagates stably in the cable sheath, and the amplitude of the stress field and displacement field gradually attenuates from near to far, which proves that the guided wave is excited and propagates in the cable sheath. The particle is selected at the excitation end of the cable sheath, and the variation curve of the circumferential displacement component of the particle with time is calculated as shown in Fig. 17.

From Fig. 17, when $t = 7.05 \times 10^{-4}$ s, the peak signal of incident wave appears in the particle, and the peak signal of end echo appears when $t = 17.3 \times 10^{-4}$ s. The time difference between the incident wave and the reflected wave of the end face is $\Delta t = 10.25 \times 10^{-4}$ s, the length of the cable section l is 0.6 m, and the wave velocity is solved by Eq. (21).

$$c = \frac{2l}{\Delta t} \tag{21}$$

The guided wave velocity is 1170.7 m/s, and the relative error with the theoretical solution is 2.34%, which satisfies the calculation accuracy.

Based on the discussion of Sections "Verification of magnetization direction of bias magnetic field and alternating magnetic field" and "Verification of torsional modal guided wave modal characteristics of cable sheath", by studying the magnetic induction intensity distribution, magnetostrictive strain signal, guided wave field distribution, axial circumferential displacement field amplitude relationship and guided wave propagation velocity at the excitation end, the validity of the model for cable sheath damage detection by exciting torsional mode guided waves under the set physical field environment, electromagnetic parameters and mechanical parameters is verified.

Parameter optimization of torsional mode guided wave excitation model

From the analysis of Section "Verification of magnetization direction of bias magnetic field and alternating magnetic field", it is known that the static bias magnetic field determines the modal characteristics of the Fe–Ni alloy with excitation guided wave, provides the structural magnetostrictive active vibration vector and effectively increases the magnetostrictive value, while the high-frequency dynamic alternating magnetic field provides the

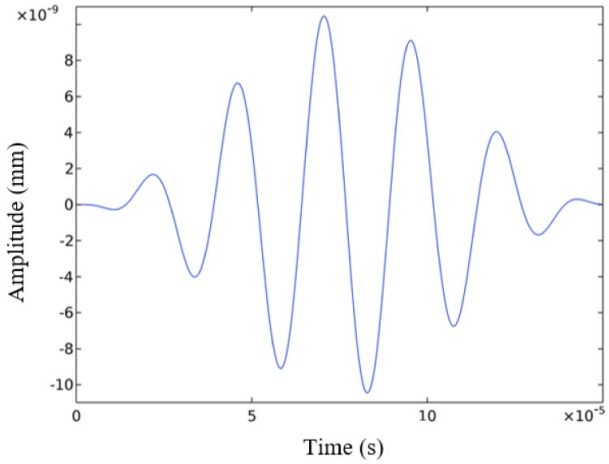

(a) Circumferential displacement component.

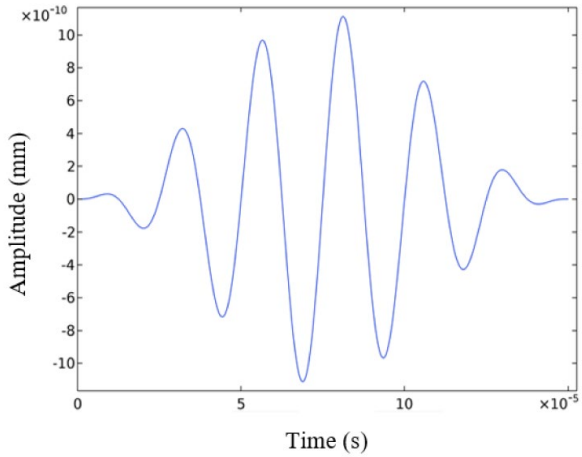

(b) Axial displacement component.

Figure 15. Torsional mode guided wave displacement signal in cable sheath. (**a**) Circumferential displacement component. (**b**) Axial displacement component.

particle guided wave. Dynamic expansion deformation, the particle generates periodic vibration and excites the guided wave under the action of superimposed magnetic field. Therefore, the pre-magnetized static bias magnetic field and the modulated dynamic alternating magnetic field are important factors affecting the vibration and propagation of particle guided waves. The high frequency dynamic magnetic field is realized by loading the alternating signal in the coil. The amplitude of the excitation current has a direct impact on the magnetic induction intensity of the dynamic magnetic field and the electromagnetic loss density of the magnetostrictive material itself, which in turn affects the mechanical response of the magnetostrictive effect.

The excitation current signal and parameter settings such as Section "Verification of magnetization direction of bias magnetic field and alternating magnetic field" are adopted. At different excitation frequencies, the relationship between the maximum dynamic flux density of the excitation coil excited by the center particle of the Fe–Ni alloy and the amplitude of the excitation current is shown in Fig. 18.

From Fig. 18, under various excitation frequencies, the magnetic flux density of the dynamic magnetic field has a linear positive correlation with the excitation current, indicating that the current intensity directly determines the magnetic induction intensity of the alternating magnetic field. When the excitation current intensity is the same, the frequency has an effect on the dynamic magnetic field flux density. The higher the frequency is, the lower the magnetic flux density is, and with the increase of current intensity, the increase of excitation frequency leads to a more obvious decrease in magnetic flux density. From the perspective of energy conversion, when the frequency increases, the particle vibrates under the action of bias magnetic field and dynamic magnetic field. The magnetostrictive amount of the particle vibration under the action of dynamic magnetic field shrinks before reaching the maximum value, resulting in a decrease in the output strain, thereby reducing the energy of guided wave vibration and propagation. Therefore, in the application process of Fe–Ni alloy strip guided wave

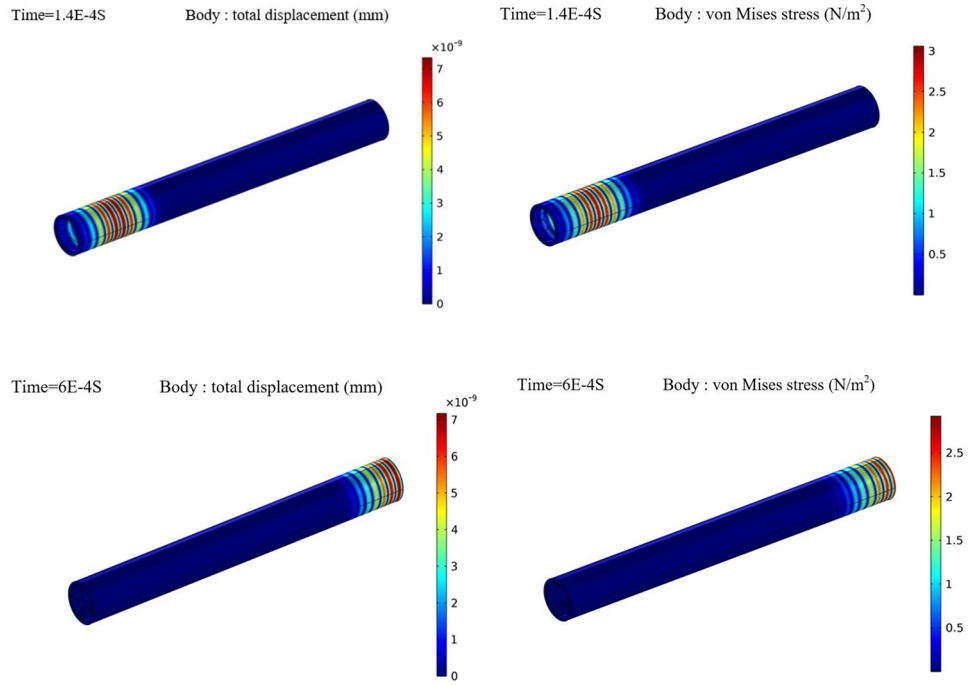

Figure 16. Displacement and stress distribution of cable sheath guided wave at different times. (**a**) The displacement and stress of cable sheath when $t = 1.4 \times 10^{-4}$ s. (**b**) The displacement and stress of cable sheath when $t = 6 \times 10^{-4}$ s.

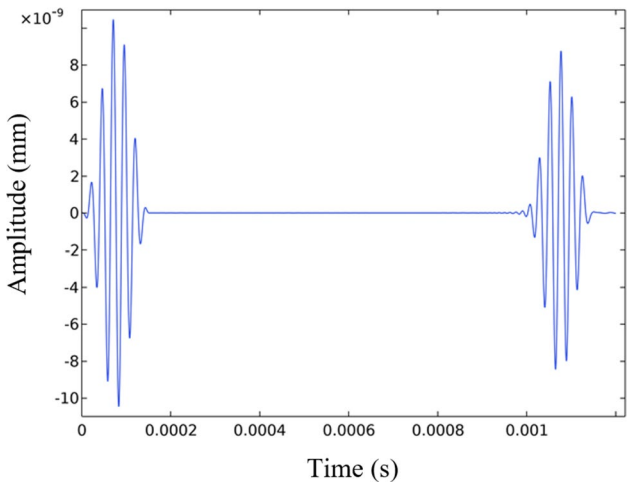

Figure 17. Circumferential displacement time history curve of cable excitation end particle.

excitation, while satisfying the working frequency (≥ 20 kHz), the lower excitation frequency is more beneficial to the energy conversion in the force-magnetic coupling process.

According to the analysis of the magnetic flux density of the dynamic magnetic field of the Fe–Ni alloy strip, with the increase of the excitation frequency, the hysteresis loss is increasing, the magnetic conductivity of the Fe–Ni alloy strip is decreasing, and the corresponding saturated magnetic field is decreasing. The excitation current is driven by the magneto-mechanical coupling effect of magnetostrictive, which finally determines the mechanical response of the coupling region, that is, the magnetostrictive strain, and finally forms a periodic stress wave for propagation. In order to ensure that the particle has enough vibration energy and output strain amplitude, and it is not appropriate to choose too large excitation current frequency in guided wave excitation, the excitation frequency is 40 kHz. Figure 19 shows the influence of different excitation current intensity on the output strain at the same frequency (40 kHz).

From Fig. 19, as the current intensity increases, the output strain increases, indicating that increasing the excitation current amplitude effectively increases the output magnetostrictive strain; however, with the increase of the amplitude of the excitation current, the output strain waveform will be distorted to varying degrees. This

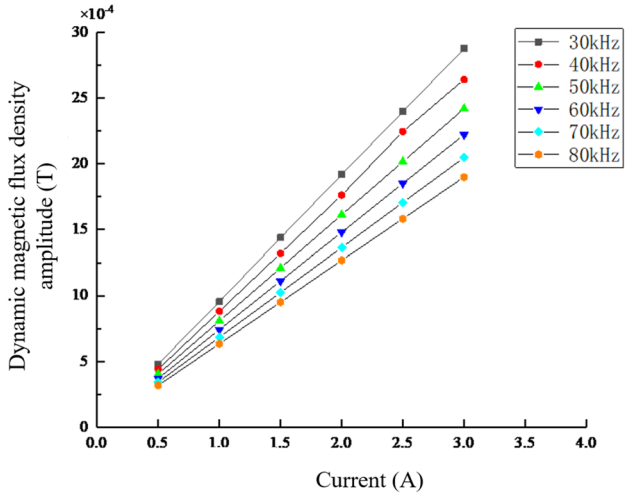

Figure 18. The variation curve of dynamic magnetic flux density amplitude with current at different frequencies.

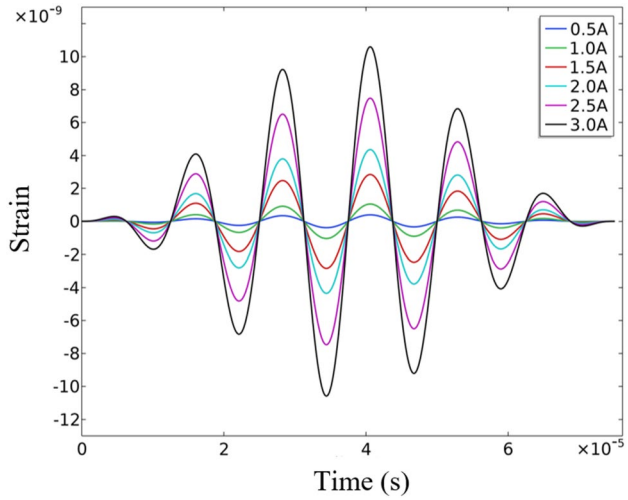

Figure 19. The curve of particle strain with time under different currents at f = 40 kHz.

is because the increase of the amplitude of the excitation current also increases the electromagnetic interference, which will reversely affect the waveform of the excitation signal, resulting in poor quality of the received waveform. At the same time, the electromagnetic loss is also increasing, and the increase is increasing. Figure 20 shows the variation curve of the electromagnetic loss of the particle under different excitation currents with time.

From Fig. 20, with the increase of current intensity, the electromagnetic loss per unit volume of Fe–Ni alloy tape is also increasing, and the electromagnetic loss is too large, which not only causes the loss of electromagnetic energy, but also causes heat, thus affecting the performance of Fe–Ni alloy tape. Combined with the output strain waveform, when ensuring that the particle has sufficient vibration energy, the appropriate excitation current amplitude should be selected to balance the magnetostrictive strain and electromagnetic density loss. Therefore, this paper chooses the current amplitude of 1A.

Simulation analysis of torsional mode guided wave detection for cable sheath damage under the influence of multiple parameters

Influence of excitation frequency on detection signal

In order to study the displacement field and damage echo characteristics of torsional guided wave in cable sheath under different excitation frequencies, the circumferential crack damage is set at 0.4 m from the left end of the cable, and the circumferential damage arc length is set to 21.54 mm, which is 10% circumferential section loss rate. The cable sheath damage is set as Fig. 21.

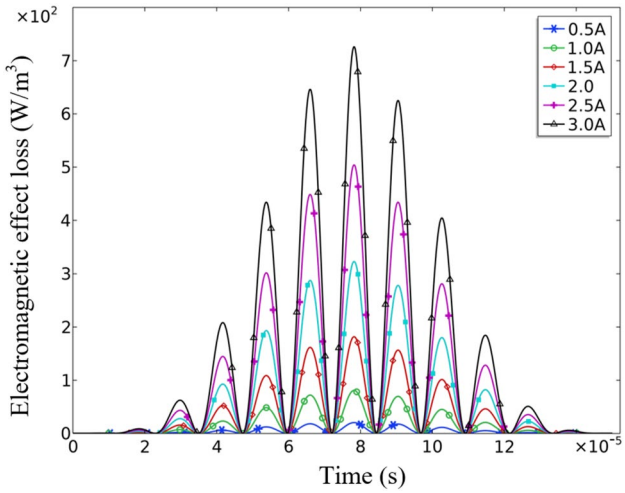

Figure 20. The variation curve of electromagnetic loss with time under different currents.

Figure 21. Cable sheath with 10% section loss rate.

The excitation frequency is selected from 40 to 80 kHz, and the step size is 10 kHz. The initial time of guided wave excitation and the time when the guided wave moves to the damaged position are taken. Under different excitation frequencies, the circumferential displacement component of the particle at the excitation end varies with time. The curve is shown in Fig. 22.

From Fig. 22, the frequency increases, the wave packet of the guided wave is more dense, but the wavelength is smaller. The smaller the wavelength is, the stronger the sensitivity of the guided wave to the variable cross section is, resulting in the weakening of its transmission capacity and the enhancement of its reflection capacity. When the frequency is 80 kHz, the torsional mode guided wave has obvious dispersion, and two modulus torsional waves are generated.

The influence of the current excitation frequency on the intensity of the guided wave is determined by the analysis method of the peak value of the echo signal. The amplitude change of the circumferential displacement component of each waveform of the guided wave under different excitation frequencies is shown in Fig. 23.

From Fig. 23, between 40 and 80 kHz, the amplitude of the reflected signal increases first and then decreases with the increase of the excitation frequency. The variation amplitude of echo amplitude between 50 and 70 kHz is only 0.6106×10^{-9} mm and 0.1260×10^{-9} mm.

In order to characterize the size of the reflected wave and the transmitted wave, the reflection coefficient R and the transmission coefficient T are defined for comparison, see Eqs. (22) and (23).

$$R = \frac{\text{Reflected wave peak}}{\text{Initial wave peak}} \tag{22}$$

$$T = \frac{\text{Transmitted wave peak}}{\text{Initial wave peak}} \tag{23}$$

The variation curves of reflection coefficient and transmission coefficient concerning the excitation frequency are shown in Fig. 24.

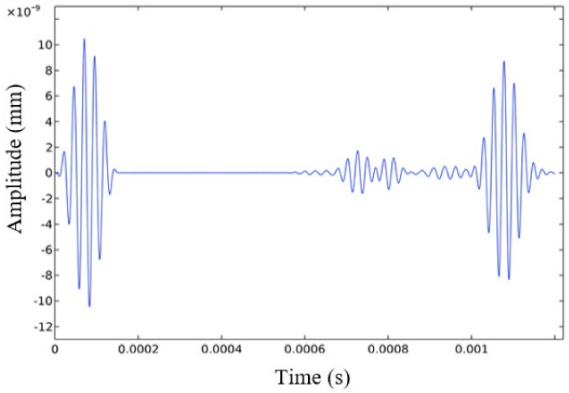

(a) 40 kHz

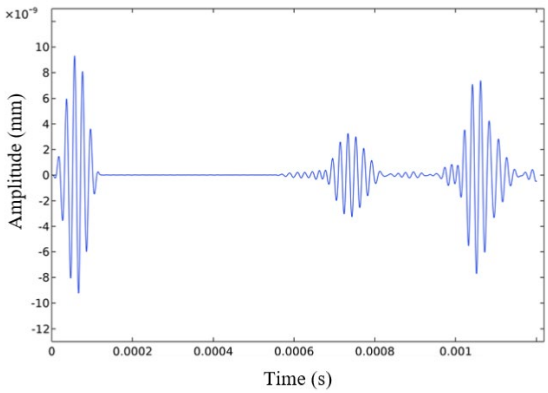

(b) 50 kHz

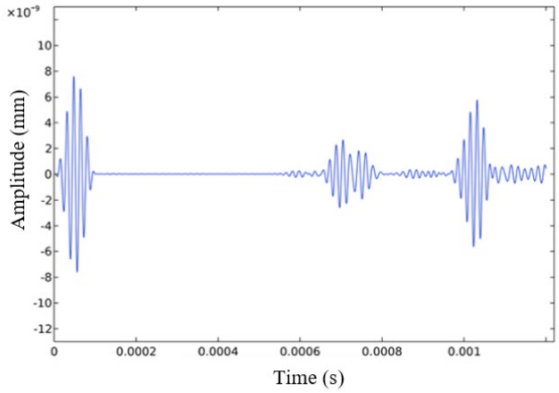

(c) 60 kHz

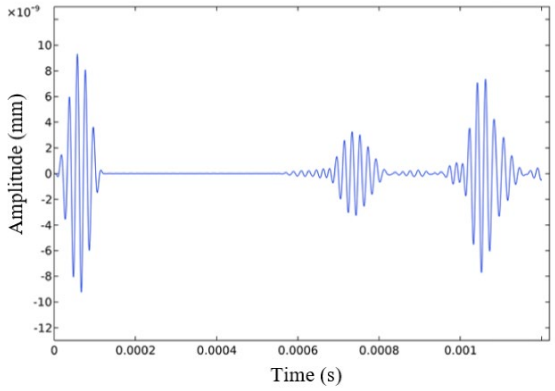

(d) 70 kHz

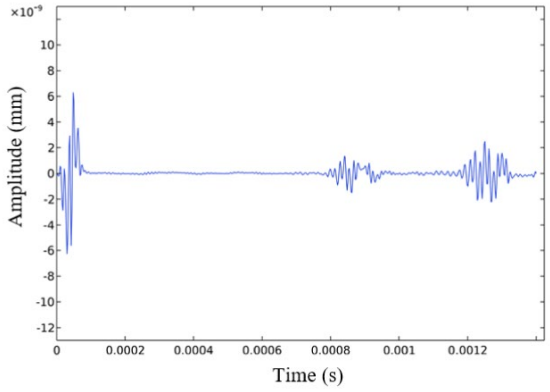

(e) 80 kHz

Figure 22. Time history curves of particle circumferential displacement at different frequencies. (**a**) 40 kHz. (**b**) 50 kHz. (**c**) 60 kHz. (**d**) 70 kHz. (**e**) 80 kHz.

From Fig. 24, when the excitation frequency increases, the reflection coefficient of the broken echo increases significantly before 50 kHz, and the increase of 50–70 kHz is small. Beyond the cut-off frequency of 75.74 kHz, the wave packet aliasing is generated, resulting in a rapid decrease in the echo coefficient. When the excitation frequency is 60 kHz, the reflection coefficient and the attenuation amplitude of the guided wave reach a balance. Observing the time-domain waveform at this time, the wave packet of the damaged reflection signal is clear.

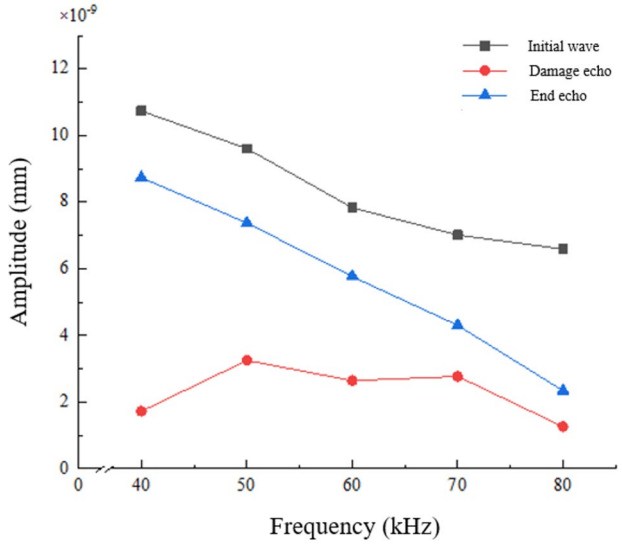

Figure 23. The amplitude of circumferential displacement component of guided wave at different frequencies.

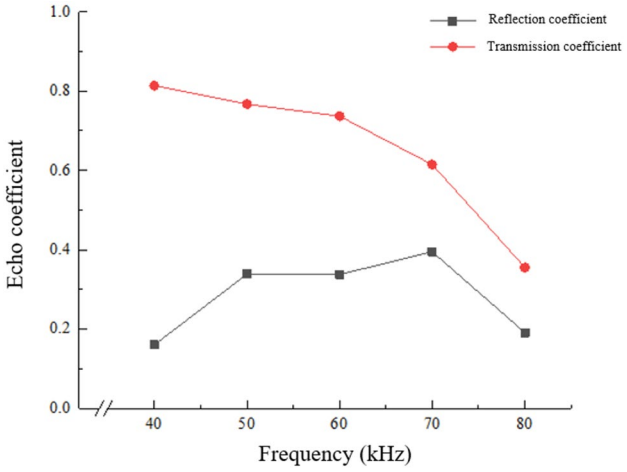

Figure 24. Dispersion curves of L and T mode guided waves.

Influence of loss rate of damaged section on detection signal

The 60 kHz excitation signal is applied, and the cross-section loss rate of the sheath is set to 5–25%. With 5% as the step size, the influence of different cross-section loss rates on the wave field characteristics of torsional guided waves is analyzed. The variation curve of the circumferential displacement component of the particle at the excitation end with time is shown in Fig. 25.

From Fig. 25, the cross-section loss rate is positively correlated with the amplitude of the damage echo, and the damage echo reaches the maximum value of 4.666×10^{-9} mm when the cross-section loss rate is 25%. The cross-section loss rate has a significant effect on the guided wave echo signal. The parameters characterizing the guided wave echo coefficient are used to quantitatively analyze the damage scale of the cable sheath. The variation of the guided wave echo peak with the cross-section loss rate is shown in Fig. 26.

From Fig. 26, the increase of damage echo increases linearly with the cross-section loss rate between 5–10% and 15–25%, and the change between 10 and 15% cross-section loss rate is not obvious. The curve of the reflection coefficient and transmission coefficient of the guided wave echo with the loss rate of the cross section is shown in Fig. 27.

The reflection coefficient presents a single value function relationship with the section loss rate. Accordingly, the reflection coefficient is selected for function fitting, to express the quantitative relationship between damaged section size and damaged echo, and evaluate the degree of sheath damage.

As shown in Fig. 28, the discrete points and fitted line residuals are approximate compared to the three function methods, and the fitting effect needs to be verified and compared by the goodness-of-fit R2 and the significance variance F. The significance variance F is 0.36, 0.03, and 0.02, which are less than 0.05, and the function fitting significance meets the requirements. Further comparison of the three functions, the R2 of the

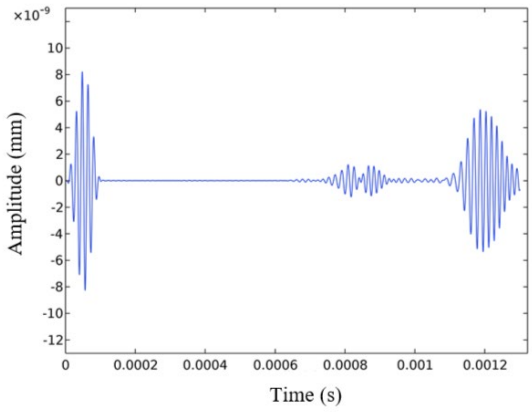

(a) 5% section loss rate

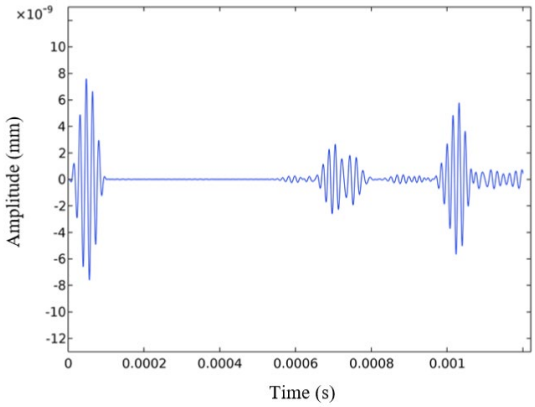

(b) 10% section loss rate

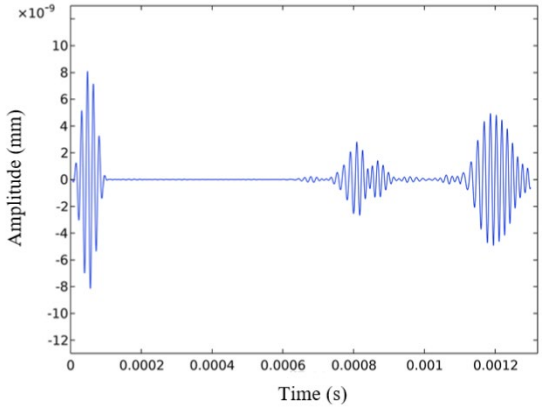

(c) 15% section loss rate

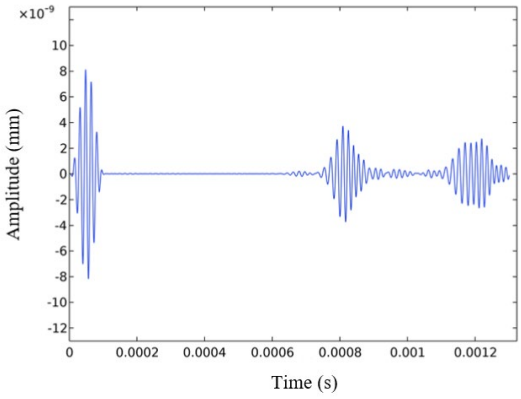

(d) 20% section loss rate

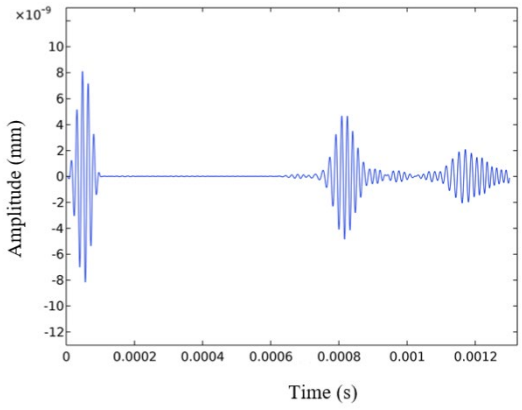

(e) 25% section loss rate

Figure 25. Time history curves of particle circumferential displacement for different section loss rates. (**a**) 5% section loss rate. (**b**) 10% section loss rate. (**c**) 15% section loss rate. (**d**) 20% section loss rate. (**e**) 25% section loss rate.

power, quadratic and cubic functions are 0.969, 0.975, and 0.978, respectively, and the explanation rate of the corresponding variables of the independent variables in the cubic function model is 97.8%, which is better goodness of fit.

The magnitude of the function variance is small when considering the three-times function fit regression estimation. The three-time fitted function was chosen as the result of the fit. The fitted function expression is Eq. (24).

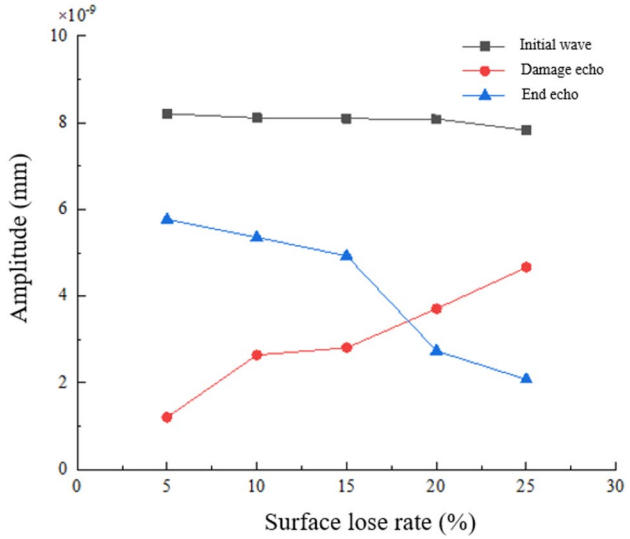

Figure 26. Amplitude of circumferential displacement component of guided wave for different section loss rates.

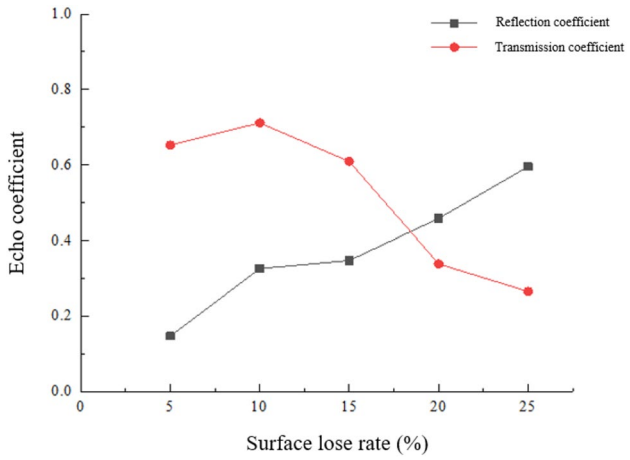

Figure 27. Curve of echo coefficient with section loss rate.

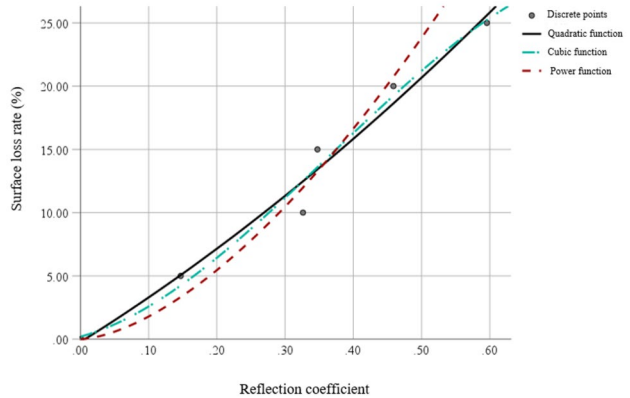

Figure 28. Fitting curve of loss rate-reflection coefficient of the damaged section.

$$y = -91.467x^3 + 100.252x^2 + 14.764x + 0.1922 \quad (24)$$

The fitting function of Eq. (24) is used as the basis for quantifying the loss rate of cable sheath damage cross-section and assessing the size of the sheath damage scale.

The effect of damage direction on the detection signal

When the excitation frequency is 60 kHz, the circumferential section loss rate is 10%. The initial damage is circumferential damage, that is, 0°. Five cross-sections with the same size as the circumferential direction of 30°, 45°, 60° and 90° are preset on the sheath.

When the damage direction changes from the circumferential direction, the torsional wave encounters the damaged section and has an obvious angle refraction phenomenon with the incident direction, and the amplitude of the guided wave returned along the incident direction is very small. The curve of the circumferential displacement component of the excitation end with time is shown in Fig. 29.

From Fig. 29, the damage angle changes, the amplitude of the particle circumferential displacement echo is greatly reduced, and the peak value of the 30° damage echo is reduced by 73.6% compared with the circumferential 0° damage. At 30°–90°, the amplitude of the damaged echo is not obvious, showing a trend of decreasing first and then increasing. The variation of the guided wave echo peak with the damage direction is shown in Fig. 30.

From Fig. 30, the damage direction between 0° and 30°, the damage echo signal is significantly reduced, and the damage echo amplitude decreases and then increases and does not change significantly between 30° and 90° cross-sectional direction, reaching the lowest at 45°, and the refraction of the torsional wave is the largest. The variation of the guided wave echo coefficient with the damage direction is shown in Fig. 31.

From Fig. 31, the angle of the broken section has a significant effect on the detection sensitivity of the torsion wave, and the reflection coefficients of 0°–90° damage are 0.3485, 0.0905, 0.0573, 0.0735, and 0.0753, which first decrease significantly with the increase of angle and increase slowly after reaching the lowest value. It indicates that the T(0,1) mode guided wave has a significant detection effect on the circumferential direction, i.e., 0° directional damage, but for the non-circumferential damage, the torsional wave mainly occurs transmission and refraction in the damage section, so the sensitivity to the damage is low. Especially for the damage in the direction of 45° from the circumferential direction, its sensitivity reaches the minimum value.

Considering the motion modal characteristics of T(0,1) guided wave, the vibration of the torsional guided waveform is in the form of circumferential vibration, and the wave propagation direction is along the sheath axial propagation, the larger the contact area between the guided wave and the damage, the stronger the reflected signal. When the damage is distributed along the circumferential direction, the contact area with the direction of wave propagation is the largest, and therefore the echo signal is the largest; conversely, when the damage is distributed along the axial direction, the detection effect is poor.

Conclusion

In this paper, the Navier displacement equilibrium equation of magnetostrictive guided wave propagation in cable sheath is established. The guided wave mode is determined by solving the dispersion curve of magnetostrictive guided wave mode. Considering the excitation frequency, loss rate of damaged section of cable sheath, and direction of damaged section, the variation in magnetostrictive guided wave displacement field in the cable sheath under the influence of multiple parameters is analyzed. Through the displacement time domain signal analysis for the echo of damaged section, the quantitative relationship between the damaged position and size of cable sheath and the guided wave excitation is studied. Finally, the following conclusions are obtained:

(1) For the first mock test of cable sheath structure, the dispersion of T mode guided waves in the frequency range of 0–200 kHz is less than that of the single mode guided waves. In the frequency range of 0–75.74 kHz, the T mode guided wave excites a single modulus T mode with group velocity and the wave velocity of guided wave in cable sheath is 1198.8 m/s.

(2) The time difference between the incident wave peak signal and the end echo peak signal of the particle at the excitation end of cable is $\Delta t = 10.25 \times 10^{-4}$ s. Meanwhile, the guided wave velocity in the simulation model is 1170.7 m/s, and the relative error with the theoretical solution is 2.34%, which ensures sufficient calculation accuracy.

(3) The magnetic flux density of the dynamic magnetic field has a linear positive correlation with different excitation currents. Under the same current, the higher the excitation frequency, the lower the magnetic flux density, and with the increase of the current intensity, the increase of the excitation frequency leads to a greater decrease in the magnetic flux density. Therefore, the lower excitation frequency is beneficial to the energy conversion in the process of magnetomechanical coupling. As the current intensity increases, the output strain increases, and the electromagnetic loss also increases, and the increase is increasing. Considering the magnetostrictive strain and electromagnetic density loss, the excitation current amplitude is selected to be 1A.

(4) With the increase of excitation frequency, the guided wave wavelength decreases, the sensitivity of guided wave to variable cross section increases, its transmission ability decreases, and its reflection ability increases. Besides, with increasing frequency, the elastic potential energy decreases when the guided wave is excited, but the guided wave energy is more concentrated. Furthermore, when the frequency is 80 kHz, the torsional mode guided wave has an obvious dispersion, and its initial wave excitation produces a torsional wave with two modules. The cut-off frequency of 75.74 kHz of T(0,1) mode is theoretically solved, and the results agree with the cut-off frequency of the medium dispersion curve T(0,1) mode i.e., 75.74 kHz.

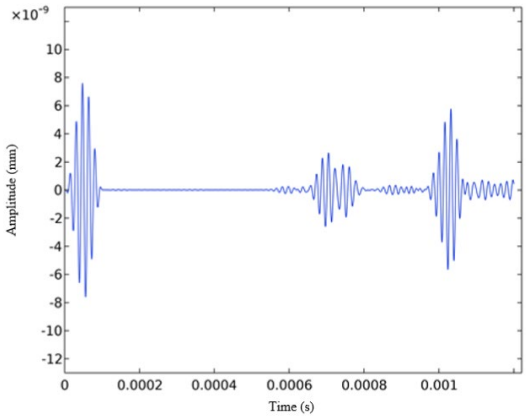

(a) 0° damage direction

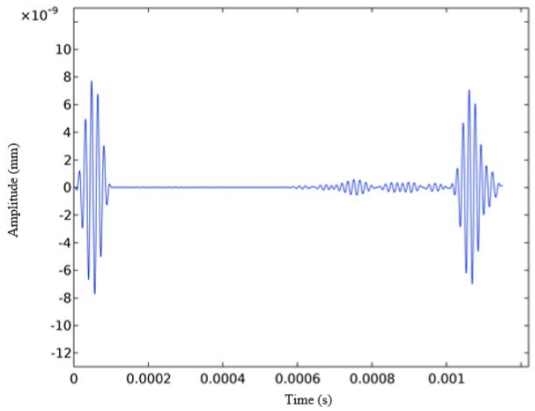

(b) 30° damage direction

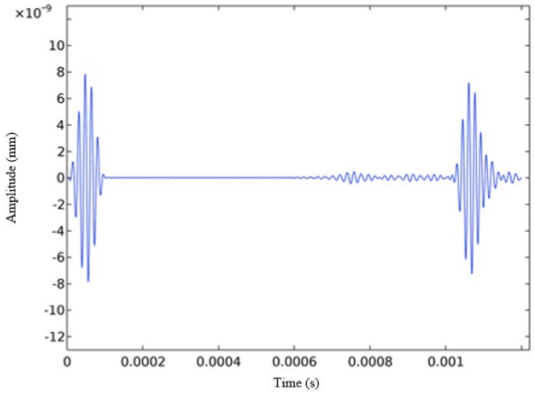

(c) 45° damage direction

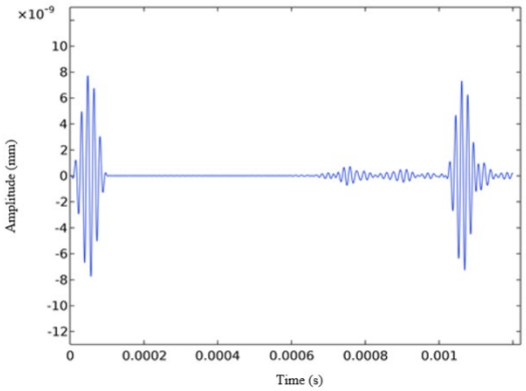

(d) 60° damage direction

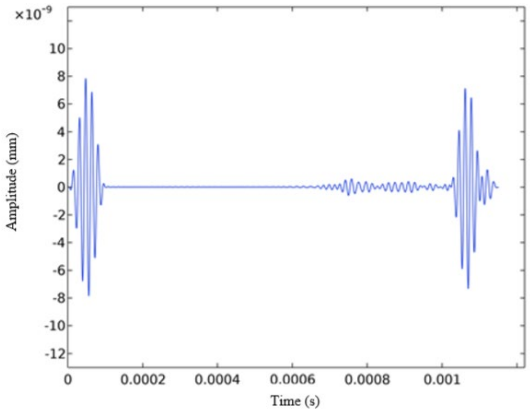

(e) 90° damage direction

Figure 29. Time history curves of circumferential displacement of particles in different damage directions. (**a**) 0° damage direction. (**b**) 30° damage direction. (**c**) 45° damage direction. (**d**) 60° damage direction. (**e**) 90° damage direction.

(5) The amplitude of damaged echo has a nonlinear positive correlation with the section loss rate, and the reflection coefficient has a single value function relationship with the section loss rate. The cubic function is used here to fit the function formula of cable sheath damaged section loss rate reflection coefficient as the basis for quantifying the cable sheath damaged section loss rate and evaluating the sheath damage scale.

(6) T(0,1) mode guided wave has a significant detection effect on circumferential damage, i.e.,0°, but for non-circumferential damage, torsional wave mainly transmits and refracts in the damaged section, hence it has

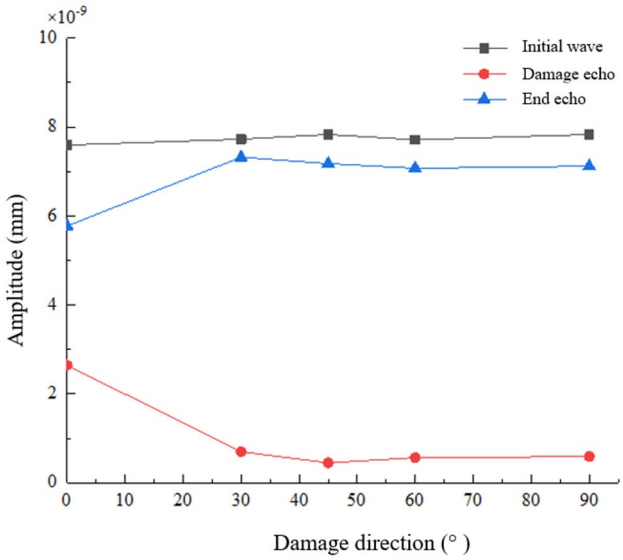

Figure 30. Variation curve of circumferential displacement component of guided wave with damage direction.

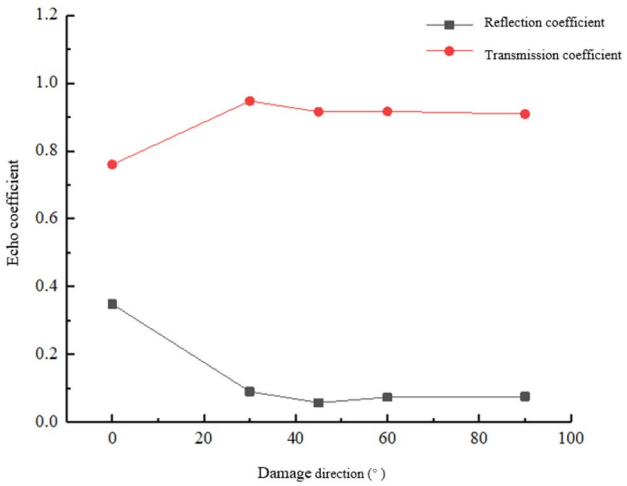

Figure 31. Curve of echo coefficient with damage direction.

low sensitivity to damage. Especially for the damage in the direction of 45° to circumferential direction, the sensitivity reaches the minimum.

Data availability

All data generated or analysed during this study are included in this published article.

Received: 13 March 2024; Accepted: 13 August 2024
Published online: 29 August 2024

References

1. Zhu, H. *et al.* Multi-factor simulation analysis of operation characteristics of side-by-side directly buried cables. *Electr. Power Syst. Res.* **218**, 109143 (2023).
2. Yang, S., Zhu, H., He, W., Yu, X. & Yuan, M. A study on structural damage of power cable jacket under external impact. *J. Vib. Shock* **39**(24), 122–127 (2020).
3. Ni, H. *et al.* Ultrasonic propagation law in 10 kV xLPE cable. *J. Appl. Acoust.* **39**(04), 589–597 (2020).
4. GB/T 28704-2012, Non-destructive testing Magnetostrictive ultrasonic waveguide detection method [S].
5. McConnell, K. U. & Zemke, W. P. The measurement of flexural stiffness of multistranded electrical conductors while under tension. *Exp. Mech.* **20**(06), 198–200 (2015).
6. Bertoncini, F., Cappelli, M., Cordella, F. & Raugi, M. An online monitoring technique for long-term operation using guided waves propagating in steel pipe. *ASME J. Nuclear Rad. Sci.* **3**(4), 041008. https://doi.org/10.1115/1.4037204 (2017).

7. Liu, Z., Zhao, J., Wu, B., Zhang, Y. & He, C. Configuration optimization of magnetostrictive transducers for longitudinal guided wave inspection in seven-wire steel strands. *NDT E Int.* **43**(6), 484–492. https://doi.org/10.1016/j.ndteint.2010.05.003 (2010).
8. Liu, Y., Wu, B., Liu, P., *et al.* Experimental study on magnetostrictive guided wave monitoring of rail bottom defects in turnout tip rails[J/OL]. Applied Acoustics 1–10 [2023–02–25]. http://kns.cnki.net/kcms/detail/11.2121.o4.20220811.1514.002.html.
9. Ghavamian, A., Mustapha, F., Baharudin, B. T. H. T. & Yidris, N. Detection, localisation and assessment of defects in pipes using guided wave techniques: A review. *Sensors* **18**, 4470. https://doi.org/10.3390/s18124470 (2018).
10. Peiwen, L. Application of magnetostrictive guided wave detection technology in long-distance pipeline crossing section[J]. *China Pet. Chem. Standard Qual.* **42**(19), 44–46 (2022).
11. Zhou, J. *Experimental research on fatigue damage detection of steel wire based on magnetostrictive guided wave [D]* (Huazhong University of Science and Technology, 2018).
12. Yang, J. *et al.* Failure detection system of pipe sheath based on magnetostrictive guided wave [J]. *Instrum. Tech. Sensor* **6**, 95–97 (2017).
13. Sun, P. Research on the mechanism and signal enhancement method of electromagnetic magnetostrictive longitudinal modal guided wave pipeline detection [D] (Huazhong University of Science and Technology, 2015).
14. Cui, Y., Zhai, Y. & Zhang, B. Application of long-distance magnetostrictive guided wave in buried pipeline detection [J]. *Chem. Equipment Technol.* **40**(05), 16–19 (2019).
15. Kam, W. J. *Research on modeling methods and influencing factors of pipeline magnetostrictive guided waves [D]* (Nanchang University of Aeronautics, 2018).
16. Cao, J. *et al. Mech. Electr. Eng.* **35**(01), 10–15 (2018).
17. Zhou, L. *et al.* Comprehensive state evaluation of high voltage cable based on multi-state characteristics and variation law [J]. *High Volt. Technol.* **45**(12), 3954–3963 (2019).
18. Yücel, M. K., Legg, M., Kappatos, V. & Gan, T. H. An ultrasonic guided wave approach for the inspection of overhead transmission line cables. *Appl. Acoust.* **122**, 23–34 (2017).
19. Yang, Z. *et al.* Damage detection of long-distance high-voltage multi-core cable sheath based on magnetostrictive guided wave [J]. *Nondestruct. Test.* **40**(12), 57–62 (2018).
20. Liu, S., Wang, S., Zhang, C., Jin, L. & Yang, Q. Simulation analysis and quantitative detection of defects of steel plate by electromagnetic ultrasonic surface wave [J]. *Chin. J. Electr. Technol.* **35**(01), 97–105 (2020).
21. Wang, Y., & Yang, B. Theory and methods of magnetostrictive guided wave nondestructive testing [M], pp. 1–43 (Science Press, Beijing, 2015).
22. Ghavamian, A., Mustapha, F., Baharudin, B. T. H. T. & Yidris, N. Detection, localisation and assessment of defects in pipes using guided wave techniques: A review. *Sensors* **18**, 4470 (2018).
23. Truong, T. D. N. *et al.* Bone-implant osseointegration monitoring using electro-mechanical impedance technique and convolutional neural network: A numerical study. *J. Nondestruct. Eval.* **43**, 10 (2024).
24. Huynh, T.-C., Lee, S.-Y., Dang, N.-L. & Kim, J.-T. Sensing region characteristics of smart piezoelectric interface for damage monitoring in plate-like structures. *Sensors* **19**, 1377 (2019).

Author contributions

He was responsible for the methodology of the manuscript, He and Cheng completed the numerical simulation and wrote the main manuscript text, Zhaobing and Wenlong processed the data of the manuscript, Zhaobing and Yue translated the manuscript.

Competing interests

The authors declare no competing interests.

Additional information

Correspondence and requests for materials should be addressed to C.L.

Reprints and permissions information is available at www.nature.com/reprints.

Publisher's note Springer Nature remains neutral with regard to jurisdictional claims in published maps and institutional affiliations.